NANO LETTERS

Letter

pubs.acs.org/NanoLett

Novel Nanostructured Paper with Ultrahigh Transparency and Ultrahigh Haze for Solar Cells

Zhiqiang Fang,[†,‡,¶] Hongli Zhu,[†,¶] Yongbo Yuan,[∥,¶] Dongheon Ha,[§] Shuze Zhu,[⊥] Colin Preston,[†] Qingxia Chen,[‡] Yuanyuan Li,[†] Xiaogang Han,[†] Seongwoo Lee,[†] Gang Chen,[‡] Teng Li,[⊥] Jeremy Munday,[§] Jinsong Huang,*[,∥] and Liangbing Hu*[,†]

[†]Department of Materials Science and Engineering, University of Maryland, College Park, Maryland 20742, United States

[‡]State Key Laboratory of Pulp and Paper Engineering, South China University of Technology, Guangzhou 510640 Guangdong, People's Republic of China

[§]Department of Electrical Engineering, University of Maryland, College Park, Maryland 20742, United States

[∥]Department of Mechanical and Materials Engineering, University of Nebraska-Lincoln, Lincoln, Nebraska 68588, United States

[⊥]Department of Mechanical Engineering, University of Maryland, College Park, Maryland 20742, United States

Supporting Information

ABSTRACT: Solar cell substrates require high optical transparency but also prefer high optical haze to increase the light scattering and consequently the absorption in the active materials. Unfortunately, there is a trade-off between these optical properties, which is exemplified by common transparent paper substrates exhibiting a transparency of about 90% yet a low optical haze (<20%). In this work, we introduce a novel transparent paper made of wood fibers that displays both ultrahigh optical transparency (~96%) and ultrahigh haze (~60%), thus delivering an optimal substrate design for solar cell devices. Compared to previously demonstrated nanopaper composed of wood-based cellulose nanofibers, our novel transparent paper has better dual performance in transmittance and haze but also is fabricated at a much lower cost. This high-performance, low-cost transparent paper is a potentially revolutionary material that may influence a new generation of environmentally friendly printed electronics.

KEYWORDS: *Light management, transparent paper, wood fibers, optical haze, solar cells*

Substrates play a key role as the foundation for optoelectronic devices. The mechanical strength, optical transparency, and maximum processing temperature are among the critical properties of these substrates that determine its eligibility for various applications. The optoelectronic device industry predominantly utilizes glass substrates and plastic substrates for flexible electronics; however, recent reports demonstrate transparent nanopaper based on renewable cellulose nanofibers that may replace plastic substrates in many electronic and optoelectronic devices.[1−11] Nanopaper is entirely more environmentally friendly than plastic substrates due to its composition of natural materials; meanwhile it introduces new functionalities due to NFCs' fibrous structure.[12−14] The maximum transparency among all current reports on glass, plastic, and nanopaper substrates is about 90% but with a very low optical haze (<20%).[15−17] Optical haze quantifies the percent of the transmitted light that diffusely scatters, which is preferable in solar cell applications.[18,19] Optical transparency and haze are inversely proportional values in various papers. Tracing paper has a high optical haze of over 50% but a transparency less than 80%, whereas plastic has a transparency of about 90% but with an optical haze of less than 1%.[20] Nanopaper based on NFCs has the highest reported optical haze among transparent substrates due to its nanoporous structure, yet it is still a relatively low value.[16]

Although optical haze is a property preferably maximized in transparent substrates integrated into solar devices, other optoelectronic devices require different levels of light scattering; for example, displays and touch screens need high clarity and low optical haze.[20,21] Current commercial substrates are best suited for displays but are not optimized for solar cell devices because of the low optical haze. Various materials such as SiO_2 nanoparticles or silver nanowires are reported to effectively increase light absorption and consequentially the short-circuit current by enhancing the path of light through the active solar layer with increased diffuse light scattering.[22−24] The light scattering induced by these nanostructures is limited, however, and incorporating these materials requires additional steps that add cost to the solar cells devices.

In this study, we report a novel transparent paper based on wood fibers, which has an ultrahigh optical transparency (~96%) and simultaneously an ultrahigh optical haze (~60%).

Received: November 4, 2013
Revised: December 8, 2013

   dx.doi.org/10.1021/nl404101p | *Nano Lett.* XXXX, XXX, XXX−XXX

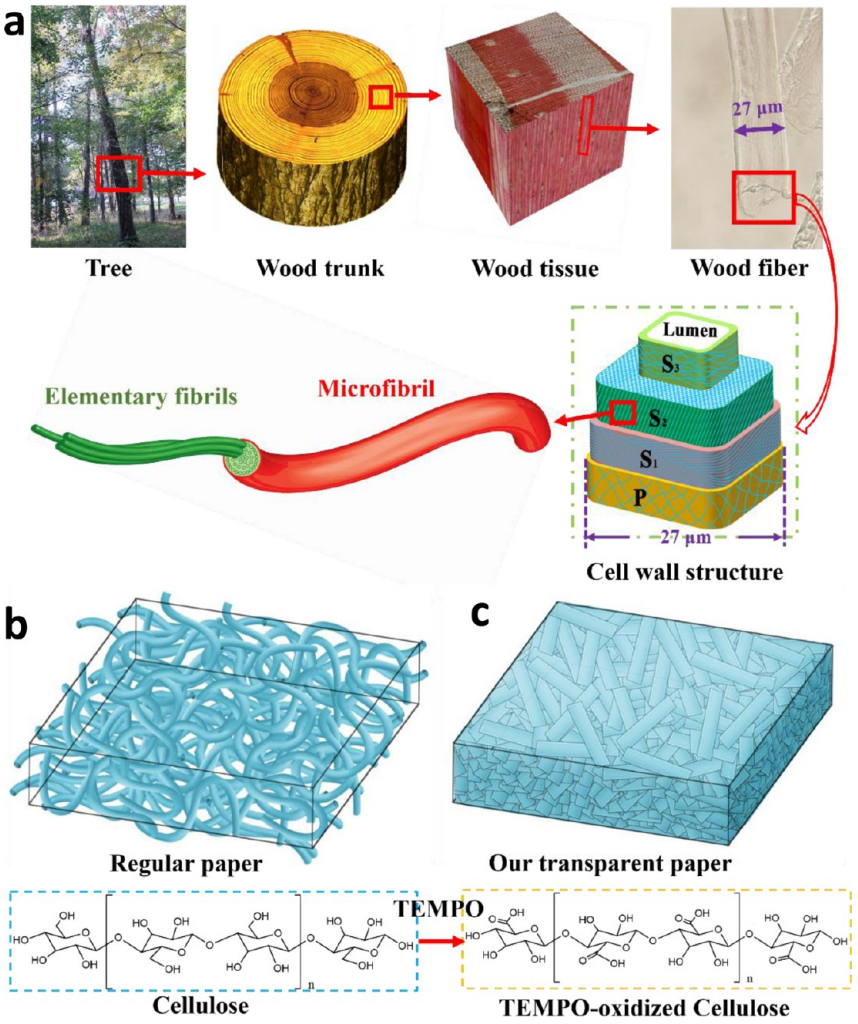

Figure 1. (a) Hierarchical structure of a tree. A schematic of cellulose and paper before and after TEMPO-mediated oxidation. (b) Top left, regular paper; bottom left, molecular structure of cellulose. (c) Top right, transparent paper made of TEMPO-oxidized wood fibers; bottom right, TEMPO-oxidized cellulose with carboxyl groups in the C6 position.

The primary wood fibers are processed by using a TEMPO/NaBr/NaClO oxidation system to introduce carboxyl groups into the cellulose. This process weakens the hydrogen bonds between the cellulose fibrils and causes the wood fibers to swell up and collapse resulting in a high packing density and excellent optical properties. Our transparent paper has the following advantages over previously reported transparent nanopaper from wood-based nanofibrillated cellulose (NFC): (1) it exhibits a dramatic dual improvement on the optical transmittance and optical haze, and (2) it is formed from much less energy intensive processes that enable low cost paper devices. The novel optical properties allow a simple light-management strategy for improving solar cell performances. We demonstrated this with an organic solar cell by simply laminating a piece of such transparent paper and observed its power conversion efficiency (PCE) increased from 5.34 to 5.88%.

Results and Discussion. A schematic of the hierarchical structure of a tree in which we gradually break down each macroscopic structure until we reach the elementary cellulose fibrils is detailed in Figure 1a. Wood fibers extracted from trees by chemical processes and mechanical treatments are the main building blocks of paper. One microfiber consists of millions of microfibrils (nanofibers) with a diameter ranging from 5 to 20 nm mainly distributed in the S2 layer of cell wall. Regular paper with microsized wood fibers has limited optical transparency due to the many microcavities existing within the porous structure that cause light scattering (top left in Figure 1b). Eliminating these pores is the primary strategy to improve the optical transmittance of paper. Many approaches based on the above mechanism are used to produce transparent paper involving fiber-based and sheet processing techniques.[26] Fiber-based methods use overbeaten wood pulp, while sheet processing requires coating, impregnating, supercalendering, or chemical immersion to make transparent paper.[26−31] These methods either consume large amounts of energy or rely on petroleum-based materials to produce paper with relatively low transmittance. Since Herrick and Turbak successfully separated nanofibers from wood pulp using a mechanical process in a high-pressure homogenizer in 1983,[32−34] cellulose nanofibers have attracted great attention because they can be used to manufacture transparent paper for printed electronics, opto-electronic devices, and also for packaging.[2,4,6,10,35−37] Some methods are used to liberate nanofibers, such as mechanical treatments and acid hydrolysis.[38−43] Mechanical treatments are currently considered efficient ways to isolate nanofibers from the cell wall of a wood fiber; however, solely mechanical processes consume large amounts of energy and insufficiently liberate the nanofibers while damaging its structures in the

dx.doi.org/10.1021/nl404101p | Nano Lett. XXXX, XXX, XXX−XXX

process.[44] Pretreatments, therefore, are conducted before mechanical disintegration in order to effectively separate the fibers and minimize the damage to the nanofiber structures.[40,45−47] TEMPO-mediated oxidation is proven to be an efficient way to weaken the interfibrillar hydrogen bonds that facilitate the disintegration of wood fibers into individualized nanofibers yet maintain a high yield of solid material.[25,44,48] Nanopaper made of nanofibers can attain a transmittance of over 80%,[15] yet this type of transparent paper takes a long time to fabricate (film forming and drying) and has a relatively low haze.[16,49]

For efficient and low-cost production of transparent paper with high transmission haze, in this study the TEMPO/NaBr/NaClO system was used to modify the surface properties of the pristine wood fibers by selectively oxidizing the C6 hydroxyl groups of glucose (left bottom in Figure 1b) into carboxyl groups under aqueous conditions (right bottom in Figure 1c). The repulsive force resulting from additional higher negative charges at the surface of the nanofibers loosens the interfibrillar hydrogen bonds between the cellulose nanofibers resulting in the fiber cell walls are significantly open and crush. Regular paper is a porous structure composed of untreated wood fibers with an average diameter of ∼27 μm (top left in Figure 1b); however, paper made from TEMPO-oxidized wood fibers with an average diameter of approximately 26 μm displays a more densely packed configuration (top left Figure 1c).

The morphology of wood fibers plays a significant role in producing highly transparent paper, hence fiber morphological analysis of TEMPO-treated wood fibers was conducted for explaining the high packing density of transparent paper made from TEMPO-oxidized microsized wood fibers. After the TEMPO treatment was conducted for 8 h at a stirring speed of 700 rpm, significant morphological changes in the dimensions of the wood fibers before and after TEMPO treatment are observed in Figure 2a,b. Compared to the original fibers, the TEMPO-oxidized fibers swell such that the width of the fibers expanded while the length decreased. Most fibers are cleaved and unzipped in the axial direction (see Figure 2c, Supporting Information Figure S2), and the degree of polymerization of the cellulose decreases.[25] Figure 2d and Supporting Information Figure S2d show the configuration of cellulose nanofibers on the cell wall of wood fibers revealing portion of cellulose nanofiber were removed from the primary layer of cell wall during the TEMPO treatment due to weak interfibrillar hydrogen bonds. As we can see from the Table 1, the average length of the wood fibers dramatically decreased from 1.98 to 0.71 mm after the TEMPO treatment, and there was a slight reduction in the average width and an enormous increase in fines (fiber length less than 200 μm) from 5.90 to 18.68%. In addition, TEMPO-oxidized wood pulp with a concentration of 0.25% (by weight) shows a more homogeneous and transparent appearance than the original wood pulp with the same consistency (see insets in Figure 2a,b). The increased fines, reduced fiber length, and the crushed and unzipped TEMPO-oxidized fibers tend to form denser fiber network during fabrication that perpetuates high optical transmittance. In this discussion, the "transparent paper" refers to paper produced from the TEMPO-oxidized wood fibers and it exhibits an excellent transmittance (see Figure2e).

In this work, a highly transparent paper with high haze was fabricated with obtained TEMPO-oxidized microsized wood fibers by vacuum filtration showing a considerable reduction of filtration time and energy. The filtration time for transparent

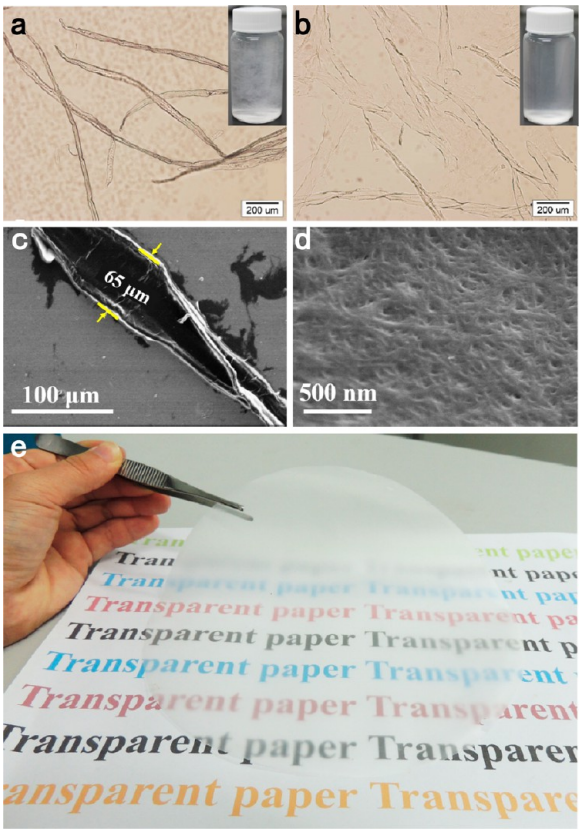

Figure 2. (a) The morphology of original bleached sulfate wood fibers under an optical microscope. Inset is a 0.25 wt % original bleached sulfate wood pulp suspension. (b) The morphology of TEMPO-oxidized wood fibers under an optical microscope. Inset is a 0.25 wt % TEMPO-oxidized wood fiber suspension. SEM images of unzipped TEMPO-oxidized wood fibers (c) and nanofibers on the cell wall of TEMPO-oxidized wood fiber (d). (e) A digital image of transparent paper produced from TEMPO-oxidized wood fibers with a diameter of 20 cm. Transparent paper is made of mesoscale fibers. The primary fibers have an average diameter of ∼26 μm.

Table 1. Dimension of Wood Fibers before and after TEMPO Oxidation

	average length (mm)	average width (μm)	fine content (%)
pristine fibers	1.98	27.25	5.90
TEMPO-oxidized fibers	0.71	25.79	18.68

paper with a thickness of 50 μm is generally less than 1 h, however it will take at least 8 h to filter a piece of nanopaper with a similar thickness using 5−30 nm wide TEMPO-oxidized nanofibers under the same conditions. The total light transmittance of transparent paper, nanopaper, and polyethylene terephthalate (PET) is compared in Figure 3a and the basic information of the two types of paper is shown in Supporting Information Table S1. According to this data, transparent paper has the highest optical transmittance compared to nanopaper and PET.

Transmission haze is an important optical property for optoelectronic devices and refers to the percentage of light diffusely scattered through a transparent surface from the total light transmitted. For the transparent paper in this work, a transmission haze over 50% is demonstrated while maintaining a transmittance of over 90%. Higher transmission haze

dx.doi.org/10.1021/nl404101p | Nano Lett. XXXX, XXX, XXX−XXX

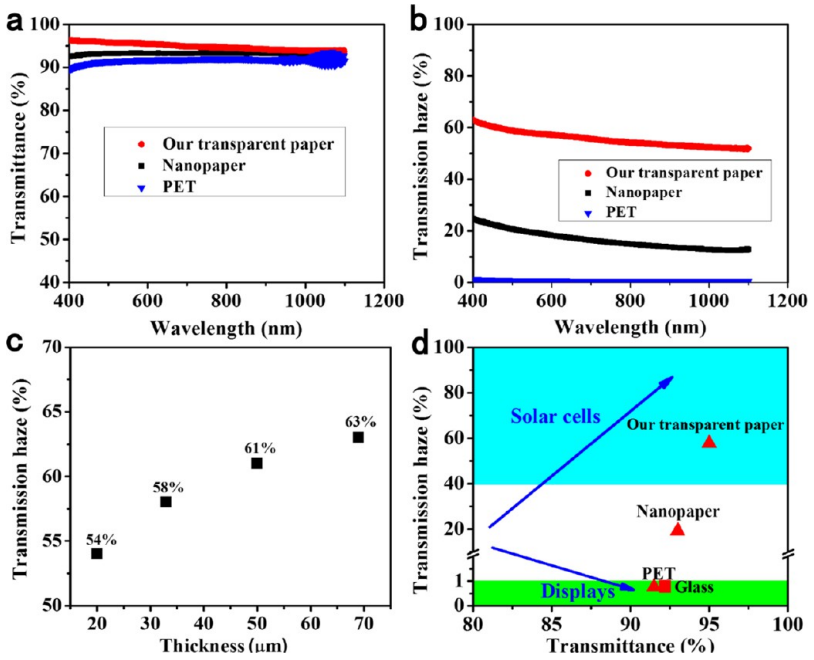

Figure 3. Optical properties of our transparent paper, nanopaper, and PET. (a) The total optical transmittance versus wavelength measured with an integrating sphere setup. (b) The transmission haze versus wavelength. (c) The transmission haze of transparent paper with varying thicknesses at 550 nm. (d) Optical transmission haze versus transmittance for different substrates at 550 nm. Glass and PET are in the green area, which are suitable for displays due to their low haze and high transparency; transparent paper developed in this work located in the cyan area is the most suitable for solar cells.

improves the light absorption efficiency of solar cells from the increased path of light transmitted into the active layer, resulting in an enhanced short circuit current density. The wavelength versus transmission haze is plotted in Figure 3b. Additionally, the transmission haze and the optical transmittance of transparent paper are also determined by the paper thickness. As we can see from Figure 3c, the transmission haze tends to increase with an increase in paper thickness while the optical transmittance increases slightly with a decrease in paper thickness (Supporting Information Figure S3 and Table S2).

It is critical to combine the optical haze and transmittance for substrates toward different applications. The performance of optical transmittance versus wavelength of substrates has been widely investigated but the optical haze is largely ignored. As shown in Figure 3d, a high clarity for substrates is crucial for displays. Glass and plastic substrates all meet this requirement. Recently developed nanopaper has an optical haze of 15−20%,[16] which is too high for display applications, but it is more suitable for solar cells.[10,50] Note some outdoor displays also requires substrates with a high haze to avoid glare under sunlight. All these substrates have an optical transmittance of ∼90%. Our transparent paper has an optical transmittance of ∼96% and transmittance haze of ∼60%, which is the most suitable substrate for solar cells.

To further explore why our transparent paper exhibits the highest transmittance, SEM images were taken to study the surface morphology of regular paper and transparent paper (Figure 4a,b respectively). Although the cylindrical wood fibers within the regular paper collapse during pressing and drying, there are plenty of cavities that form throughout the network of microsized fibers causing enhanced light scattering behavior due to the refractive index mismatch between cellulose (1.5) and air (1.0). In Figure 4b, a homogeneous and more conformal surface is observed due to the collapse of the TEMPO-oxidized wood fibers and there is a significant amount of small fragments in the pulp that fill in the voids within the paper (see the insert in Figure 4b). This causes less light scattering to occur within the TEMPO-treated paper and allow more light to pass through it.

A possible explanation for the transparent paper demonstrating a higher optical transmittance than nanopaper could be that the cell wall of the wood fibers are comprised of a primary and secondary layer with thicknesses of approximately 0.1−0.2 and 1−5.5 μm, respectively.[51] The microfibrils are randomly oriented in the primary layer whereas the microfibrils in the secondary layer are helically wound around the fiber axis (see Figure 1a). Although oxidation effectively weakens the interfibrillar hydrogen bonds between the microfibrils and shortens fiber length, it only happens within the noncrystalline region and/or on the crystal surfaces of the microfibrils.[44] As a result, the parallel arrangement of microfibrils in the secondary layer is preserved within the cell wall of the wood fibers, giving rise to a higher stacking density (1.14 g/cm^3) compared to nanopaper (1.03 g/cm^3) made of randomly arranged microfibrils. Transparent paper made of microsized fibers, therefore, has better optical transmittance yet consumes much less energy and time for fabrication.

Additionally, the mechanical properties of paper (e.g., toughness, strength) are important for various applications. To this end, we conducted tensile tests of the transparent paper with TEMPO-oxidized wood fibers and regular paper using the Tinius Olsen H25KT universal testing machine. The comparison between their stress−strain curves (Figure 4c) clearly shows that the transparent paper is both much stronger (with a tensile strength of ∼105 MPa) and much tougher (with a toughness of ∼1.88 J/M^3) than the regular paper (with a tensile strength of ∼8 MPa and a toughness of ∼0.15 J/M^3). With regard to the influence of paper's density on its

dx.doi.org/10.1021/nl404101p | Nano Lett. XXXX, XXX, XXX−XXX

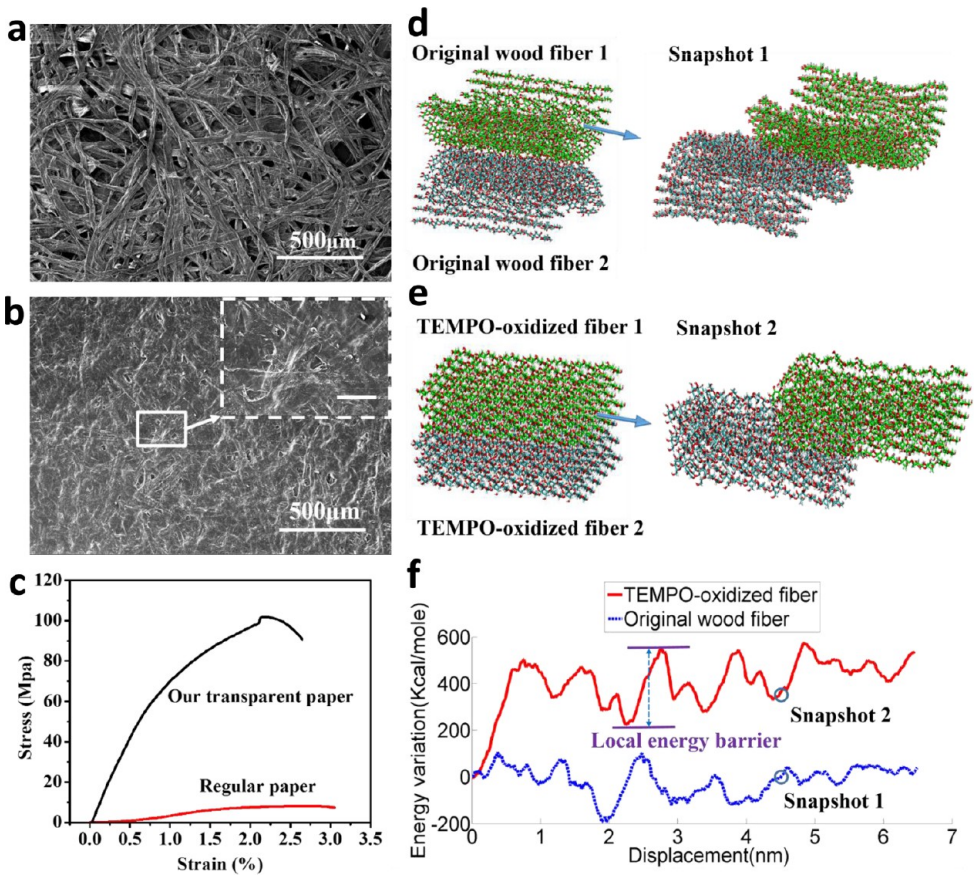

Figure 4. Top-view SEM images of (a) regular paper and (b) transparent paper. The insert in top right corner is a magnified SEM image of transparent paper where the scale bar is 100 μm. (c) The tensile strength of transparent paper demonstrated in this work and regular paper. MD simulation model of intersliding of (d) two original wood fibers and (e) two TEMPO-oxidized wood fibers. Videos of these two simulations are available in Supporting Information. (f) Variation of potential energy of the model systems as a function of relative sliding displacement for both cases.

mechanical properties, the specific strength verses strain curves of regular paper compared to transparent paper are in the Supporting Information (Figure S4a). These improvements in the mechanical properties (~13-fold stronger and ~12-fold tougher than regular paper) are the result of enhanced contact area in between nanoscale building blocks of the paper. This greater surface area is caused by the TEMPO-treatment and its effect is two-fold: unzipping and cleaving the originally hollow cellulose fibers not only exposes their inner surface to neighboring fibers but also forms ribbon-like cellulose flakes and fragments that facilitate higher packing density and more overlapping between neighboring fibers. The numerous hydroxyl groups on the cellulose surface allow facile formation of strong hydrogen bonds. The intercellulose-flake bonding in TEMPO-oxidized transparent paper is expected to be consequently much stronger than the intercellulose-fiber bonding in regular paper, and is the origin of the substantial improvements in both strength and toughness.

To shed quantitative insight on the above mechanism, we performed molecular dynamics (MD) simulations of scaled-down models for both TEMPO-oxidized fibers and original wood fibers with roughly comparable size (Figure 4d,e and Supporting Information Figure S4b,c). Note that the simulation is based on simplified fiber with uniform dimension but fiber morphology, fines content, kink index, and pigments within paper are some properties that may impact the mechanical strength of paper. We simulated the interflake (and interfiber) sliding, the representative molecular-scale deformation mechanism that leads to the final mechanical failure of the paper (detailed mechanical modeling information and simulation videos are found in the Supporting Information). Figure 4f compares the variation of potential energy as a function of sliding displacement for both cases. The zigzag nature of the curve denotes the cascade stick−slip events due to breaking and reforming of hydrogen bonds in between two cellulose flakes (or fibers) under sliding displacement. The accumulated energy dissipation, calculated by the sum of all local energy barriers, represents the energy to fracture the neighboring flakes/fibers (i.e., toughness). Comparison in Figure 4f reveals that the energy needed to separate two flat cellulose flakes is more than 14 times higher than that in the case of two cellulose fibers (~536 kcal/mol vs ~38 kcal/mol), which clearly explains the huge increase in fracture toughness due to TEMPO treatment. The resultant force variation as a function of sliding displacement for both cases is showed in Supporting Information Figure S4d. The required average pulling force to slide the TEMPO-oxidized cellulose flakes (~−284 kcal/mol/Å) is much larger than that in the original cellulose fiber case (−66 kcal/mol/Å). Considering the effective reduction of the cross-sectional area from the hollow cellulose fibers to TEMPO-treated flat flakes, the mechanical strength of TEMPO-oxidized cellulose paper (largest force that can sustain divided per unit cross-section area) is expected to be even

dx.doi.org/10.1021/nl404101p | Nano Lett. XXXX, XXX, XXX−XXX

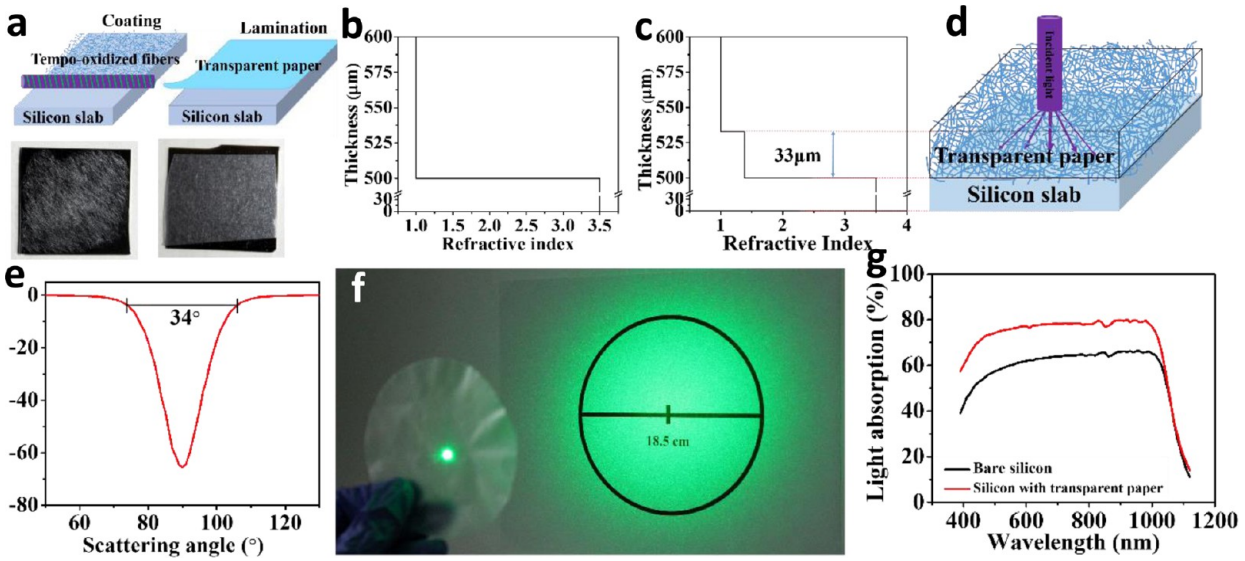

Figure 5. (a) Schematics and images of cellulose-deposited silicon slab. Top left: a schematic structure of wood fibers deposited on a silicon slab by Meyer rod coating. Top right: a schematic of a transparent paper attached silicon slab by lamination. Bottom left: TEMPO-oxidized wood fibers deposited on a silicon slab. Bottom right: transparent paper with a thickness of 33 μm attached on a silicon slab. (b) The effective refractive index profiles of the interfaces between air and silicon slab. (c) The effective refractive index profiles of 33 μm cellulose deposited on a silicon slab. (d) A schematic diagram of transparent paper and its light scattering behavior. (e) Scattering angular distribution with an arbitrary *y*-axis unit for transparent paper, the maximum scattering angle is 34°. (f) Photo to show the light scattering effect of transparent paper when a laser with a diameter of 0.4 cm passes though transparent paper. (g) The light absorption of transparent paper laminated on a silicon slab.

higher than that of regular paper, as revealed by the tensile test results (Figure 4c).

Paper with ultrahigh transmittance and high transmission haze has potential applications in optoelectronic devices. The light scattering effect of transparent paper can improve the path of light traveling through the active layers of thin film solar cells resulting in an enhanced light absorption. To verify the assumption, TEMPO-oxidized wood fibers directly coated onto the surface of a silicon slab and transparent paper laminated onto the surface of silicon using NFC as a binder to analyze any resulting enhancement of light absorption in the silicon. Schematics and images of the cellulose-deposited silicon are shown in Figure 5a, where the left plots refer to the TEMPO-oxidized wood fiber deposited silicon, and the right diagrams represent transparent paper-laminated silicon. There are three possible mechanisms to achieve increased light absorption in the active layer: (1) the index of transparent paper is between the values for the Si substrate and air, which can effectively decrease the index contrast and lower the reflection for light entering from air to Si (compare Figure 5b and 5c); (2) a large light forward scattering effect of transparent paper, which can increase the path length of light in the Si layer (as shown in Figure 5d); (3) a ultrahigh optical transparency up to 96% of our transparent paper. These effects make transparent paper fundamentally better than plastic substrates for thin film solar cells.

As shown in the schematic Figure 5d, the direct incident light is scattered as it propagates through the transparent paper, generating a high transmission haze. To quantitatively explain the light scattering effect of transparent paper, an optical setup consisting of a rotating light detector was applied to measure the angular distribution of transmitted light. Light passing through transparent paper exhibits high diffuse scattering with an expected inverse Gaussian-like pattern (Figure 5e). Here, we define the angle that the incident light is perpendicular to the surface of transparent paper as 90° and the scattering angle range is defined as the transmitted light at angles with an intensity larger than 5% of the peak transmission intensity at 90°. Our transparent paper delivers a maximum scattering angle of 34°. Moreover, the distribution of light transmitted through the transparent paper demonstrated in this work is quite different from nanopaper (as shown in Supporting Information Figure S5) since the transmitted light has a much narrower angular distribution. The light scattering effect is also visualized in Figure 5f (the distance between the transparent paper and target is about 30 cm). A laser with a wavelength of 532 nm and a beam diameter of 0.4 cm passes through transparent paper and forms a larger illuminated circular area on the surface of the target with a diameter of over 18.5 cm. The same experiment was also applied to glass and PET to illustrate the light scattering effect, and the results are presented in Supporting Information Figure S6. Because the transmission haze of PET and glass is lower than 1%, the transmitted light is scattered only slightly as visualized by a smaller illuminated area on the target behind the transparent paper. Figure 5g illustrates the light absorption of transparent paper laminated on a silicon slab. The data on the light absorption of TEMPO-oxidized wood fibers deposited on silicon is very similar and is shown in Supporting Information Figure S7. Compared to a bare silicon slab, there is enhanced light trapping in all the prepared samples by approximately 10−18% from 400 to 1000 nm. These results show that (1) both TEMPO-oxidized wood fibers and transparent paper can enhance the broadband absorption efficiency of the silicon slab, and (2) transparent paper or TEMPO-treated wood fibers can be applied to a silicon slab with a simple coating, dipping, or lamination that depends on the specific application desired.

In addition, the light harvesting of the OPV device can also be improved by simply attaching the transparent paper to the glass side of the OPV sample, as illustrated in Figure 6a. On the opposite side, OPV device with a structure of indium tin oxide (ITO)/poly(3, 4-ethylenedioxythiophene)-polystyrenesulfonic

dx.doi.org/10.1021/nl404101p | *Nano Lett.* XXXX, XXX, XXX−XXX

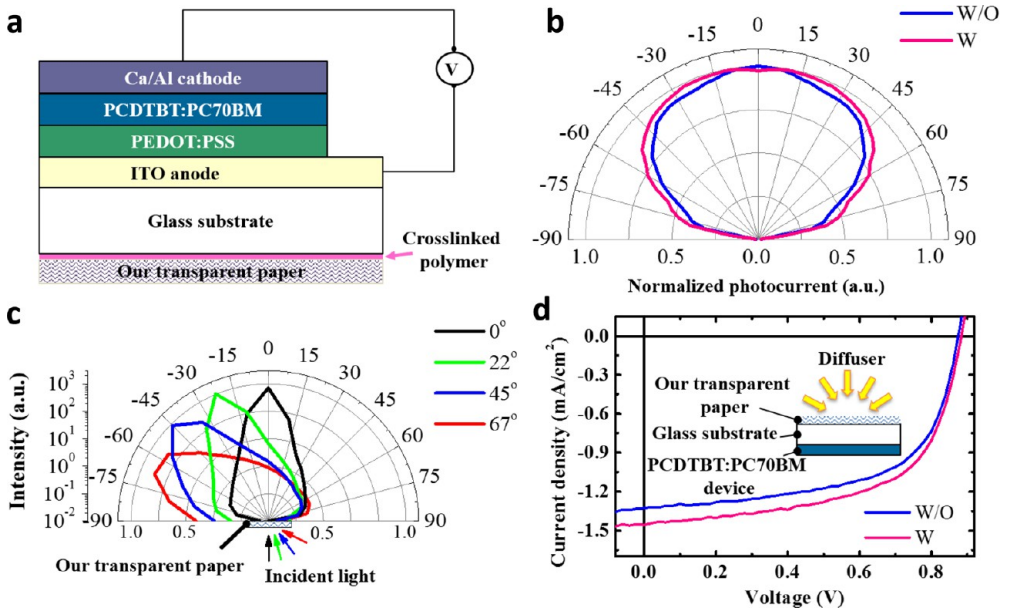

Figure 6. Enhanced light harvesting in the OPV device by the transparent paper. (a) Structure of the OPV device with transparent paper attached on the opposite glass side. (b) Dependence of the photocurrent of the OPV device with or without transparent paper on the light incident angle (defined as the angle between the incident light and the normal direction of the substrate), W and W/O represent OPV device with and without transparent paper, respectively. (c) Angular distribution of the light caused by the haze effect of the transparent paper, where the light was incident at different angle. (d) Comparison of the *I*–*V* curves of the OPV device illuminated by diffused light (13 mW/cm^2).

acid (PEDOT-PSS)/Poly[*N*-9″-hepta-decanyl-2, 7-carbazole-alt-5,5-(4′,7′-di-2-thienyl-2′,1′,3′-benzothiadiazole)] and [6,6]-phenyl-C71 butyric acid methyl ester (PCDTBT:PC70BM, 90 nm)/calcium (Ca)/aluminum (Al) has been previously fabricated,[52] and the molecular structures of the photoactive materials for the OPV device are indicated in Supporting Information Figure S8. It is expected that the haze effect of the transparent paper causes the incident angle-dependent photocurrent response. To verify this, the photocurrents of the devices under illumination from different incident angles were measured by illuminating the devices with parallel white light and rotating the devices gradually. The measured incident angle-dependent photocurrents are shown in Figure 6b. Here the incident angle is defined as the angle between the incident light and the normal direction of the substrate. The photocurrent has been normalized to the values obtained from the control device (without transparent paper) with light incident to the normal direction. The photocurrent of the device with transparent paper was about 3% less than that of the control device at the normal incident direction, most likely due to the roughly 90% diffusive transmittance of the transparent paper.[16] Interestingly, the photocurrents of the device with transparent paper exceed that of the control device at a larger incident angle above 7°. A large photocurrent improvement of over 15% were observed in an incident angle range of 60∼87°. The improved photocurrent should be correlated with the reduced reflection of the light at glass surface and a broadened angular distribution of the redirected incident light caused by the transparent paper, as shown in Figure 6c. Similar antireflection effects have been observed in solar cells with microstructure arrays or a textured surface.[53−55]

The increased light harvesting at oblique incidence indicates that the device with transparent paper can collect the ambient light more efficiently. In order to further demonstrate the improved ambient light harvesting by the transparent paper, we compared the PCE of the device illuminated by diffused light with intensity of 13 mW/cm^2, and the setup is illustrated in the inset of the Figure 6d. The PCE of the PCDTBT:PCBM device with transparent paper was increased from 5.34 to 5.88% due to the increased photocurrent by 10% (Figure 6c). The performance improvement is attributed to better light harvesting from the diffused light because the *I*–*V* curves were obtained from the same OPV device upon attaching or peeling off the transparent paper. The increased ambient light harvesting by the transparent paper is particularly desirable for many photovoltaic applications, such as in application that cannot use mechanical light tracking systems to compensate for shift in the incident sunlight throughout the day like solar roofs, solar windows, and solar panels working in cloudy days where the sunlight is strongly scattered by the atmosphere.

In summary, this study is the first report of a novel transparent paper substrate made of earth-abundant wood fibers that simultaneously achieves an ultrahigh transmittance (∼96%) and ultrahigh optical haze (∼60%), and its optimal application on the solar cells with a PCE enhancement of 10% by a simple lamination process. The modified wood pulp with high fragment content and fewer hollow structures lead to a higher packing density, which dramatically increases both the optical transmittance and mechanical strength of our transparent paper compared to regular paper. Our transparent paper demonstrates a much higher optical transmittance than nanopaper made of nanoscale fibers while using much less energy and time to process paper with a similar thickness. Such low-cost, highly transparent, and high haze paper can be utilized as an excellent film to enhance light-trapping properties for photovoltaic applications such as solar panel, solar roof, or solar windows.

Experimental Section. Bleached sulfate softwood pulp extracted from the southern yellow pine without beating or refining was treated with TEMPO-oxidized system.[15,48] Five grams of wood fibers were dispersed into 1% pulp with deionized water. TEMPO and sodium bromide (NaBr) were

dx.doi.org/10.1021/nl404101p | *Nano Lett.* XXXX, XXX, XXX−XXX

then separately added into the wood pulp with doses of 10 and 1.6 wt % based on oven-dry wood fibers, and the mixtures were finally stirred continuously for 10 min at 700 rpm with a Turrax mixer (IKA, RW20 digital) to form a uniform suspension. Thirty-five milliliters of sodium hypochlorite (NaClO) with a concentration of 12.5 wt % was titrated into the above-mentioned suspension. The reaction time was monitored and the pH of the reaction system was kept constant at 10.5. The reaction lasted approximately 3−4 h; however, the mixture was continuously stirred at 700 rpm for an additional 4 h to ensure adequate reaction of the wood fibers. The dimension and morphology of the wood pulp before and after oxidation was tested using a KajaaniFS300 fiber analyzer and an optical spectroscope (OLYMPUS BX51).

NFC (nanofibrillated cellulose) with a diameter of approximately 5−30 nm used for the fabrication of nanopaper was extracted from the above-mentioned TEMPO-oxidized wood fiber solution using a Microfluidizer processor (M110 EH, Microfluidics Inc., U.S.A.). The treated wood pulp was pumped once through thin z-shaped chambers with channel dimension of 200 μm in the Microfluidizer under a process pressure of 20 000 psi.

The treated wood pulp was diluted to approximately 0.2 wt % in solution with deionized water. This diluted pulp was then used to fabricate transparent paper by a filtration method using a 20 cm filter membrane (0.65 μm, PVDF). The resulting wet film was placed between two stacks of regular filter paper and dried at room temperature under pressure. The optical properties of the paper were measured using a UV−vis Spectrometer Lambda 35 containing an integrating sphere (PerkInElmer, U.S.A.).

Six hundred microliters of wood fiber dispersion with a consistency of 1 wt % was coated onto a 1 cm^2 silicon slab and dried at room temperature. To measure the optical properties of this sample, we built a custom optical setup. A xenon light source was used with a monochromator to select specific wavelengths from 400 to 1000 nm with a 10 nm step size. By comparing the amount of light entering the integrating sphere to the amount of light exiting the integrating sphere, the total absorption was measured. Two separate measurements are made: one baseline measurement with no sample in place to calibrate the system and a second measurement with the sample. By considering the difference between these two measurements, the absorptivity of the sample was calculated.

For the device fabrication, a 30 nm thick PEDOT:PSS layer was fabricated on a cleaned ITO/glass substrate by spin-coating with a rotating speed of 3500 rpm. The spun PEDOT:PSS film was then baked at 130 °C for 15 min. PCDTBT:PC70BM dissolved in 1, 2-dichlorobenzene with a blending ratio of 1:2 (by weight) was used for the spin-coating of photoactive layer. The active layer obtained by spin-coating with a rotating speed of 2400 rpm for 20 s has a thickness of approximately 90 nm. Then the Ca/Al bilayer cathode was thermally deposited in succession. When attaching the transparent paper on the glass surface for a better light coupling from the transparent paper to the glass, as well as strong adhesion, a cross-linked polymer (ethoxylated bisphenol A dimethacrylate mixed with 1 wt % 2,2-dimethoxy-2-phenylacetophenone[56]) was formed between the transparent paper and the glass substrate.

■ ASSOCIATED CONTENT

Ⓢ Supporting Information

Detail information of the dimension and morphology of wood fibers before and after TEMPO-oxidized treatment, optical transmittance of our transparent paper with different thickness, specific strength and mechanical modeling of our transparent paper, scattering angular distribution of nanopaper, light-scattering effect of PET and glass, light absorption of TEMPO-oxidized wood fibers deposited silicon slab, and molecular structure of materials used in OPV devices. This material is available free of charge via the Internet at http://pubs.acs.org.

■ AUTHOR INFORMATION

Corresponding Authors

*E-mail: (L.H.) binghu@umd.edu.
*E-mail: (J.H.) jhuang2@unl.edu.

Author Contributions

[¶]Z.F., H.Z., and Y.Y. contributed equally.

Notes

The authors declare no competing financial interest.

■ ACKNOWLEDGMENTS

This project was supported by Air Force Office of Scientific Research (AFOSR) Investigator Program. Z.F. would like to thank the China Scholarship Council (CSC) for financial support. We acknowledge the support of the Maryland NanoCenter and its NispLab. The NispLab is supported in part by NSF as a MRSEC (Materials Research Science and Engineering Center) Shared Experimental Facility. We would also like to acknowledge the Biotechnology Research and Education Program for letting us use their Microfluidizer and to thank Joseph Murray for help with the optical setup. J.H. would like to acknowledge the National Science Foundation under Awards ECCS-1201384 and ECCS-1252623. T.L. and Z.S. acknowledge the support of the National Science Foundation (Grant Numbers 1069076 and 1129826).

■ REFERENCES

(1) Nakagaito, A. N.; Nogi, M.; Yano, H. *MRS Bull.* **2010**, *35*, 214−218.
(2) Nogi, M.; Iwamoto, S.; Nakagaito, A. N.; Yano, H. *Adv. Mater.* **2009**, *21* (16), 1595−1598.
(3) Nogi, M.; Yano, H. *Appl. Phys. Lett.* **2009**, *94* (23), 233117−233117−3.
(4) Huang, J.; Zhu, H.; Chen, Y.; Preston, C.; Rohrbach, K.; Cumings, J.; Hu, L. *ACS Nano* **2013**, *7* (3), 2106−2113.
(5) Zhu, H.; Xiao, Z.; Liu, D.; Li, Y.; Weadock, N. J.; Huang, J.; Hu, L.; Fang, Z. *Energy Environ. Sci.* **2013**, *6* (7), 2105−2111.
(6) Nogi, M.; Komoda, N.; Otsuka, K.; Suganuma, K. *Nanoscale* **2013**, *5*, 4395−4399.
(7) Nogi, M.; Yano, H. *Adv. Mater.* **2008**, *20* (10), 1849−1852.
(8) Zheng, G.; Cui, Y.; Karabulut, E.; Wagberg, L.; Zhu, H.; Hu, L. *MRS Bull.* **2013**, *38* (4), 320−325.
(9) Hu, L.; Liu, N.; Eskilsson, M.; Zheng, G.; McDonough, J.; Wågberg, L.; Cui, Y. *Nano Energy* **2013**, *2* (1), 138−145.
(10) Hu, L. B.; Zheng, G. Y.; Yao, J.; Liu, N. A.; Weil, B.; Eskilsson, M.; Karabulut, E.; Ruan, Z. C.; Fan, S. H.; Bloking, J. T.; McGehee, M. D.; Wagberg, L.; Cui, Y. *Energy Environ. Sci.* **2013**, *6* (2), 513−518.
(11) Zhang, W.; Zhang, X.; Lu, C.; Wang, Y.; Deng, Y. *J. Phys. Chem. C* **2012**, *116* (16), 9227−9234.
(12) Missoum, K.; Belgacem, M. N.; Bras, J. *Materials* **2013**, *6* (5), 1745−1766.

(13) Missoum, K.; Belgacem, M. N.; Barnes, J.-P.; Brochier-Salon, M.-C.; Bras, J. *Soft Matter* **2012**, *8* (32), 8338−8349.
(14) Missoum, K.; Bras, J.; Belgacem, M. N. *Cellulose* **2012**, *19* (6), 1957−1973.
(15) Fukuzumi, H.; Saito, T.; Iwata, T.; Kumamoto, Y.; Isogai, A. *Biomacromolecules* **2008**, *10* (1), 162−165.
(16) Zhu, H.; Parvinian, S.; Preston, C.; Vaaland, O.; Ruan, Z.; Hu, L. *Nanoscale* **2013**, *5* (9), 3787−3792.
(17) Siró, I.; Plackett, D.; Hedenqvist, M.; Ankerfors, M.; Lindström, T. *J. Appl. Polym. Sci.* **2011**, *119* (5), 2652−2660.
(18) Chiba, Y.; Islam, A.; Watanabe, Y.; Komiya, R.; Koide, N.; Han, L. *Jpn. J. Appl. Phys., Part 2* **2006**, *45* (24/28), L638.
(19) Berginski, M.; Hupkes, J.; Schulte, M.; Schope, G.; Stiebig, H.; Rech, B.; Wuttig, M. *J. Appl. Phys.* **2007**, *101* (7), 074903−074903−11.
(20) MacDonald, W. A.; Looney, M. K.; MacKerron, D.; Eveson, R.; Adam, R.; Hashimoto, K.; Rakos, K. *J. Soc. Inf. Disp.* **2007**, *15* (12), 1075−1083.
(21) Hecht, D. S.; Thomas, D.; Hu, L.; Ladous, C.; Lam, T.; Park, Y.; Irvin, G.; Drzaic, P. *J. Soc. Inf. Disp.* **2009**, *17* (11), 941−946.
(22) Jeong, S.; Hu, L.; Lee, H. R.; Garnett, E.; Choi, J. W.; Cui, Y. *Nano Lett.* **2010**, *10* (8), 2989−2994.
(23) Kang, G.; Park, H.; Shin, D.; Baek, S.; Choi, M.; Yu, D. H.; Kim, K.; Padilla, W. J. *Adv. Mater.* **2013**, *25* (18), 2617−2623.
(24) Chung, C. H.; Song, T. B.; Bob, B.; Zhu, R.; Duan, H. S.; Yang, Y. *Adv. Mater.* **2012**, *24* (40), 5499−5504.
(25) Saito, T.; Isogai, A. *Biomacromolecules* **2004**, *5* (5), 1983−1989.
(26) Reyden, D. v. d.; Hofmann, C.; Baker, M. *J. Am. Inst. Conserv.* **1993**, *32* (2), 177−206.
(27) Koike, T.; Amano, M. Transparent cellulosic paper and method for making the same. U.S. Patent 4137046 A, 1979.
(28) Castle, W. J.; Mehta, R. Method of transparentizing a cellulose substrate. U.S. Patent 6692819 B1, 2004.
(29) Simcoke, D. R. Transparentized paper and method for its manufacture. Patent WO1991001882 A1, 1991.
(30) Bachmann, K. *Book Paper Annu.* **1983**, *2*, 3−13.
(31) Nishino, T.; Arimoto, N. *Biomacromolecules* **2007**, *8* (9), 2712−2716.
(32) Turbak, A. F.; Snyder, F. W.; Sandberg, K. R. In *Microfibrillated Cellulose, a New Cellulose Product: Properties, Uses, and Commercial Potential*; ITT Rayonier Inc.: Shelton, WA, 1983.
(33) Turbak, A. F.; Snyder, F. W.; Sandberg, K. R. Microfibrillated cellulose. U.S. Patent 3701484, 1983.
(34) Herrick, F. W.; Casebier, R. L.; Hamilton, J. K.; Sandberg, K. R. In *Microfibrillated Cellulose: Morphology and Accessibility*; ITT Rayonier Inc.: Shelton, WA, 1983.
(35) Okahisa, Y.; Yoshida, A.; Miyaguchi, S.; Yano, H. *Compos. Sci. Technol.* **2009**, *69* (11−12), 1958−1961.
(36) Nogi, M.; Iwamoto, S.; Nakagaito, A. N.; Yano, H. *Abstr. Pap. Am. Chem. Soc.* **2009**, 237.
(37) Belbekhouche, S.; Bras, J.; Siqueira, G.; Chappey, C.; Lebrun, L.; Khelifi, B.; Marais, S.; Dufresne, A. *Carbohydr. Polym.* **2011**, *83* (4), 1740−1748.
(38) Abdul Khalil, H. P. S.; Bhat, A. H.; Ireana Yusra, A. F. *Carbohydr. Polym.* **2012**, *87* (2), 963−979.
(39) Moon, R. J.; Martini, A.; Nairn, J.; Simonsen, J.; Youngblood, J. *Chem. Soc. Rev.* **2011**, *40* (7), 3941−3994.
(40) Isogai, A.; Saito, T.; Fukuzumi, H. *Nanoscale* **2011**, *3* (1), 71−85.
(41) Siró, I.; Plackett, D. *Cellulose* **2010**, *17* (3), 459−494.
(42) Wang, Q. Q.; Zhu, J. Y.; Reiner, R. S.; Verrill, S. P.; Baxa, U.; McNeil, S. E. *Cellulose* **2012**, *19* (6), 2033−2047.
(43) Dong, X. M.; Revol, J.-f.; Gray, D. G. *Cellulose* **1998**, *5* (1), 19−32.
(44) Saito, T.; Okita, Y.; Nge, T. T.; Sugiyama, J.; Isogai, A. *Carbohydr. Polym.* **2006**, *65* (4), 435−440.
(45) Saito, T.; Nishiyama, Y.; Putaux, J.-L.; Vignon, M.; Isogai, A. *Biomacromolecules* **2006**, *7* (6), 1687−1691.
(46) Saito, T.; Kimura, S.; Nishiyama, Y.; Isogai, A. *Biomacromolecules* **2007**, *8* (8), 2485−2491.
(47) Nakagaito, A. N.; Yano, H. *Appl. Phys. A: Mater. Sci. Process.* **2004**, *78* (4), 547−552.
(48) Isogai, A.; Kato, Y. *Cellulose* **1998**, *5* (3), 153−164.
(49) Sehaqui, H.; Liu, A. D.; Zhou, Q.; Berglund, L. A. *Biomacromolecules* **2010**, *11* (9), 2195−2198.
(50) Zhou, Y.; Fuentes-Hernandez, C.; Khan, T. M.; Liu, J.-C.; Hsu, J.; Shim, J. W.; Dindar, A.; Youngblood, J. P.; Moon, R. J.; Kippelen, B. *Sci. Rep.* **2013**, *3*, 1536.
(51) Huang, C. L.; Lindström, H.; Nakada, R.; Ralston, J. *Holz Roh-Werkst.* **2003**, *61* (5), 321−335.
(52) Park, S. H.; Roy, A.; Beaupré, S.; Cho, S.; Coates, N.; Moon, J. S.; Moses, D.; Leclerc, M.; Lee, K.; Heeger, A. J. *Nat. Photonics* **2009**, *3* (5), 297−302.
(53) Zhao, J.; Wang, A.; Green, M. A.; Ferrazza, F. *Appl. Phys. Lett.* **1998**, *73*, 1991.
(54) Zhao, J.; Wang, A.; Campbell, P.; Green, M. A. *IEEE Trans. Electron Devices* **1999**, *46* (7), 1495−1497.
(55) Zhou, W.; Tao, M.; Chen, L.; Yang, H. *J. Appl. Phys.* **2007**, *102* (10), 103105−103105.
(56) Yu, Z.; Zhang, Q.; Li, L.; Chen, Q.; Niu, X.; Liu, J.; Pei, Q. *Adv. Mater.* **2011**, *23* (5), 664−668.